

Diagnosing excited state quantum phase transition with multiple quantum coherence spectrum in the Lipkin-Meshkov-Glick model

Qian Wang

*Department of Physics, Zhejiang Normal University, Jinhua 321004, China and
CAMTP-Center for Applied Mathematics and Theoretical Physics,
University of Maribor, Mladinska 3, SI-2000 Maribor, Slovenia*

Francisco Pérez-Bernal

*Departamento de Ciencias Integradas y Centro de Estudios Avanzados en Física,
Matemáticas y Computación, Universidad de Huelva, Huelva 21071, Spain and
Instituto Carlos I de Física Teórica y Computacional, Universidad de Granada, Granada 18071, Spain
(Dated: October 12, 2022)*

We use the multiple quantum coherence (MQC) spectrum to explore the effects of excited-state quantum phase transition (ESQPT) on the quantum coherence in the Lipkin-Meshkov-Glick (LMG) model—a paradigmatic model in the studies of ESQPTs. MQC spectrum is calculated with respect to a given reference basis and applied to both evolved and long time averaged states. We show that the MQC spectrum undergoes an abrupt change as the system passes through ESQPT, indicating a strong impact of ESQPT on quantum coherences. We further discuss the ability of zero mode of MQC spectrum to probe the presence of ESQPT and verify that it behaves as a reliable indicator of ESQPT. In addition, we perform an investigation on the behavior of MQC spectrum width. We find that the MQC spectrum widths for both evolved and long time averaged states are act as good ESQPT witnesses. Our results provide further evidence to confirm the usefulness of the MQC spectrum for diagnosing different types of phase transitions in many-body quantum systems.

I. INTRODUCTION

The extension of the ground state quantum phase transition [1, 2] to the excited states leads to the so-called excited-state quantum phase transition (ESQPT) [3–5]. Unlike the ground state quantum phase transitions, which concern the non-analytical change in the ground state properties, the ESQPTs are focused on an abrupt change in the nature of higher-energy eigenstates. ESQPTs are usually manifested by closing gaps between excited states at the critical energy, which gives rise to the singularities in the density of states. Hence, the presence of ESQPTs are usually identified through the behavior of the density of states [5, 6].

ESQPTs have been theoretically verified in various many-body quantum systems [5], including Lipkin-Meshkov-Glick (LMG) model [7–11], Dicke and Rabi model [12–15], spinor Bose-Einstein condensates [16, 17], molecular bending transitions [18–20], periodically driven systems [21, 22], interacting boson model [23, 24], coupled top model [25, 26], as well as Kerr nonlinear oscillators [27]. Moreover, ESQPTs were also experimentally observed in microwave Dirac billiards [28, 29] and spin-1 Bose-Einstein condensates [30]. Both the static and dynamical effects of ESQPT have been revealed in numerous studies [31–50]. In addition, the investigation of ESQPTs in the systems with quantum chaos further unveils the correlations between ESQPT and the onset of chaos [22, 51–53]. Recently, the role of ESQPT in the thermalization process for the isolated many-body quantum systems has also been analyzed [54, 55]. However, to the best of our knowledge, the analysis of how ESQPT affects the quantum coherence is still an open question,

although there have several studies discuss the impacts of ESQPT on decoherence process in different many-body quantum systems [32–34].

As one of conerstones of quantum theory, quantum coherence plays an important role in various applications of current quantum technologies [56]. The quantum coherence developed in quantum state is fully characterized by the multiple quantum coherence (MQC) spectrum. The concept of the MQC spectrum was first introduced in the context of nuclear magnetic resonance and has long been regarded as a measure of quantum coherence [57–59]. Very recently, it has also been used as a witness of entanglement [60–64] and quantum phase transitions in many-body quantum systems [65, 66]. Further application of the MQC spectrum includes the description of the evolutions of correlations [67, 68] and the diagnosis of localization transitions [69–71].

In this work, we use the MQC spectrum to systematically investigate the effects of ESQPT on the quantum coherence in the Lipkin-Meshkov-Glick (LMG) model. By varying the energy of the system, the LMG model undergoes an ESQPT which characterized by logarithmic divergence of the density of states at the critical energy. The divergence in the density of state is a consequence of the unstable fixed point appearing in the dynamics of the classical limit of the LMG model. We show that the occurrence of ESQPT leads to a drastic change in the MQC spectrum for both time evolved and long time averaged states. We further illustrate how to identify the signatures of ESQPT from the behavior of the zero mode of MQC spectrum. In particular, we demonstrat that the width of the MQC spectrum stands as a reliable ESQPT witness. The aim of our study is to provide a detailed

exploration of the mutual relationship between ESQPT and quantum coherence and to show the usefulness of the MQC spectrum for detecting ESQPT in many-body quantum system.

The article is structured as follows. In Sec. II, we begin with a brief review to the concept of MQC spectrum. In Sec. III, we present the LMG model and its classical limit, mainly focus on the characters of ESQPT. Our main results are given in Sec. IV. Specifically, in Sec. IV A we discuss the MQC spectrum of the evolved state after a quench, and we reveal the signatures of ESQPT in the properties of the MQC spectrum width in Sec. IV B. Then, in Sec. IV C we study the MQC spectrum of the long time averaged state. We finally summarize our results and conclude in Sec. V.

II. MULTIPLE QUANTUM COHERENCE SPECTRUM

The MQC spectrum is the spectra of the MQC intensities. The definition of MQC intensity requires to choose some reference basis, as the quantum coherence depends on the choice of basis. To this end, let us consider a Hermitian operator \mathcal{O} with $|\nu_n\rangle$ being its eigenstates and ν_n the corresponding eigenvalues, such that $\mathcal{O}|\nu_n\rangle = \nu_n|\nu_n\rangle$. An arbitrary quantum state ρ can be decomposed in the basis $\{|\nu_n\rangle\}$ as follows

$$\rho = \sum_{\ell} \rho_{\ell}, \quad (1)$$

where ρ_{ℓ} denotes the ℓ th block of the density matrix and takes the form

$$\rho_{\ell} = \sum_{\nu_n - \nu_m = \ell} \rho_{nm} |\nu_n\rangle \langle \nu_m|, \quad (2)$$

with $\rho_{nm} = \langle \nu_n | \rho | \nu_m \rangle$. The block ρ_{ℓ} is the so-called ℓ coherence which possesses all coherences between n th and m th eigenstates of \mathcal{O} that satisfy $\nu_n - \nu_m = \ell$. The ℓ th MQC intensity quantifies the ℓ coherence and defines as the Frobenius norm (or Schatten 2-norm) of the ℓ th block [64–66],

$$I_{\ell}(\rho) \equiv (\|\rho_{\ell}\|_2)^2 = \text{Tr}[\rho_{\ell}^{\dagger} \rho_{\ell}]. \quad (3)$$

Then the set of $I_{\ell}(\rho)$ for different values of ℓ , denoted by $\{I_{\ell}(\rho)\}$, gives the MQC spectrum of the state ρ with respect to \mathcal{O} . The width of the MQC spectrum is measured by its second moment, which behaves as a lower bound of quantum Fisher information [64] and is defined as

$$\Sigma(\rho, \mathcal{O}) = \left[\sum_{\ell} \ell^2 I_{\ell}(\rho) \right]^{1/2}. \quad (4)$$

It has been demonstrated that the MQC spectrum and its second moment are useful QPT witnesses in both Hermitian [65] and non-Hermitian many-body quantum systems [66]. The advantage of studying the MQC spectrum is that it can be directly accessed in a variety of

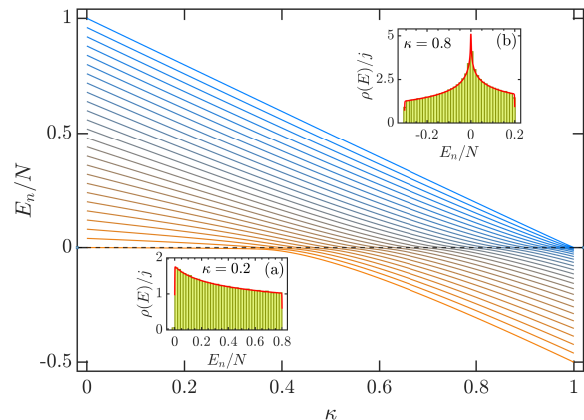


FIG. 1. Normalized energy spectrum of the LMG Hamiltonian (5) as a function of κ with $j = N/2 = 25$. The dashed horizontal line indicates the critical energy $E_c = 0$. In the insets we plot the rescaled density of states for $\kappa < \kappa_c$ (a) and $\kappa > \kappa_c$ (b) with $N = 5000$ and $\kappa_c = 1/3$. The red solid line in each inset represents the classical result $\rho_{cl}(E)$ in Eq. (11) (see main text). The axes in all figures are dimensionless.

experimental platforms [63, 65]. Moreover, the experimental measurement of the MQC spectrum requires minimal cost comparing with other indicators of QPT, such as Loschmidt echoes [72] and quantum fidelity [73].

In the following, we will assess the MQC spectrum for the LMG model and mainly focus on how to unveil the signatures of ESQPT through the properties of the MQC spectrum. We will show that the MQC spectrum serves as a useful diagnostic tool to detect the presence of ESQPT.

III. LIPKIN-MESHKOV-GLICK MODEL

The LMG model was first developed in the nuclear physics [74] and nowadays it becomes a paradigmatic model in the studies of various quantum phase transitions [3, 5, 75–84], quantum thermodynamics [46, 85–88], quantum metrology [89–91], quantum control [92–94], and quantum information [95–100], to name a few. It has also been employed to explore the effect of unstable stationary point on the spreading of out-of-time order correlators [101], the behavior of the complexity in the system with infinite range interaction [102], and the existence of Floquet time-crystal in the system without disorder [103]. Importantly, it can be realized in many of current state-of-the-art experiments [104–108].

As the fully connected Ising model, the LMG model describes an ensemble of N mutually interacting spin-1/2 particles with the Hamiltonian given by

$$H = -\frac{2\kappa}{N} J_x^2 + (1 - \kappa) \left(J_z + \frac{N}{2} \right), \quad (5)$$

with $0 \leq \kappa \leq 1$. Here, κ is the strength of interaction between spins, and $J_{x,y,z} = \sum_{i=1}^N \sigma_i^{x,y,z}$ are the collective

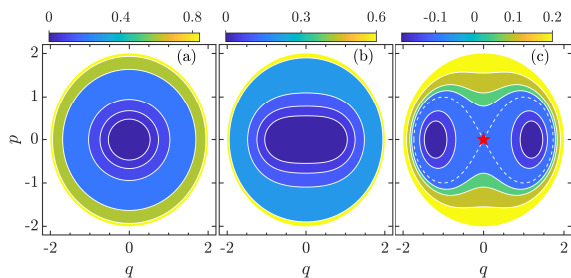


FIG. 2. Contour plots of the energy surface of the classical Hamiltonian (10) for $\kappa = 0.3\kappa_c$ (a), $\kappa = \kappa_c$, and $\kappa = 2\kappa_c$. The red star and dashed line in panel (c) denote the saddle point and the corresponding separatrix in phase space, respectively. Other parameter: $\kappa_c = 1/3$. The axes in all figures are dimensionless.

spin operators with $\sigma_i^{x,y,z}$ are the Pauli matrices acting on the i th site. Here and throughout this work, we set $\hbar = 1$.

The conservation of the total spin operator $\mathbf{J}^2 = J_x^2 + J_y^2 + J_z^2$ and the parity operator $\Pi = e^{i\pi(j+J_z)}$ for the Hamiltonian (5) allows us to restrict our study to the subspace $j = N/2$ with even-parity, leading the Hilbert space reduces to a dimension $\mathcal{D}_{\mathcal{H}} = N/2 + 1$. The Hamiltonian (5) can be diagonalized within the Dicke states $|m\rangle$ defined as $J_z|m\rangle = m|m\rangle$, where the quantum number $j = N/2$ has been dropped for brevity and $-j \leq m \leq j$.

The ground state of Hamiltonian (5) undergoes a second-order quantum phase transition at $\kappa_c = 1/3$, which separates the ferromagnetic phase ($\kappa < \kappa_c$) from the paramagnetic phase ($\kappa > \kappa_c$). The signatures of this ground state phase transition have been thoroughly investigated in literature [80–85, 109–111]. In addition, it is known that Hamiltonian (5) also shows an ESQPT for $\kappa > \kappa_c$ at the critical energy $E_c = 0$ [3, 5, 10, 31, 33]. In this work, we focus on how to characterize this ESQPT through the multiple quantum coherence.

ESQPTs are signified by the singularity in the density of states, due to the clustering of energy levels at the critical energy [3, 5]. This is illustrated for the LMG model in the main panel of Fig. 1, where we plot the normalized energy spectrum as a function of control parameter κ . Meanwhile, in the insets of Fig. 1, we show the density of states, defined as $\rho(E) = \sum_n \delta(E - E_n)$, for $\kappa < \kappa_c$ and $\kappa > \kappa_c$ cases, respectively. Clearly, in contrast to the simple behavior observed in the inset (a) for $\kappa < \kappa_c$, the collapse of energy levels around $E_c = 0$ for $\kappa > \kappa_c$ case leads to a sharp peak in the density of states [see inset (b)]. Moreover, the sharp density of states peak at $E_c = 0$ will transform into a logarithmic divergence in the thermodynamic limit [3, 6], implying that the ESQPT in the LMG model can be characterized by singularity in the density of states [9–11, 33], as expected.

The emergence of ESQPT in the LMG model can be understood by studying its classical limit ($j \rightarrow \infty$). To derive the classical version of Hamiltonian (5), we first

consider its expectation value with respect to spin coherent state [112, 113]

$$|\xi\rangle = \frac{1}{(1 + |\xi|^2)^j} e^{\xi J_+} |j, -j\rangle, \quad (6)$$

where $\xi \in \mathbb{C}$ is a parameter, $J_{\pm} = J_x \pm iJ_y$ are the spin raising and lowering operators, and $|j, -j\rangle$ is the eigenstate of J_z , that is $J_z|j, -j\rangle = -j|j, -j\rangle$. By employing the following relations [112]

$$\begin{aligned} \langle \xi | J_+ | \xi \rangle &= \frac{2j\xi^*}{1 + |\xi|^2}, & \langle \xi | J_- | \xi \rangle &= \frac{2j\xi}{1 + |\xi|^2}, \\ \langle \xi | J_z | \xi \rangle &= j \left(\frac{|\xi|^2 - 1}{|\xi|^2 + 1} \right), \end{aligned} \quad (7)$$

one can easily find that the expectation value of the LMG Hamiltonian in spin coherent state is given by

$$\begin{aligned} \mathcal{H}_c(\xi) &= \frac{\langle \xi | H | \xi \rangle}{N} \\ &= -\frac{\kappa(\xi + \xi^*)^2}{2(1 + |\xi|^2)^2} + (1 - \kappa) \frac{|\xi|^2}{1 + |\xi|^2}. \end{aligned} \quad (8)$$

Then, by parameterizing ξ in terms of the classical canonical variables (p, q) as

$$\xi = \frac{q + ip}{\sqrt{4 - (p^2 + q^2)}}, \quad (9)$$

we arrive at the classical Hamiltonian of the LMG model, which reads as

$$\mathcal{H}_c(p, q) = -\frac{\kappa q^2}{8}(4 - p^2 - q^2) + \frac{1 - \kappa}{4}(p^2 + q^2). \quad (10)$$

The fixed points of $\mathcal{H}_c(p, q)$ are the solutions of $\nabla \mathcal{H}_c(p, q) = 0$ and given by

$$(p, q)_f = \begin{cases} (0, 0), & \kappa \leq \kappa_c, \\ \left(0, \pm \sqrt{\frac{3\kappa - 1}{\kappa}} \right), & \kappa > \kappa_c. \end{cases}$$

The associated energy for these fixed points are

$$\mathcal{E}_f = \begin{cases} 0, & \text{for } \kappa \leq \kappa_c, \\ -\frac{(3\kappa - 1)^2}{8\kappa}, & \text{for } \kappa > \kappa_c. \end{cases}$$

Fig. 2 shows the contour plots of the energy surface of the classical LMG model for several values of κ . In Fig. 2(a), we observe that the energy surface has circular contours with a global minimum at the original point $(0, 0)$ for small κ . At $\kappa = \kappa_c$, the global minimum is still at the center of the energy surface but the contours start to display deformation, as shown in Fig. 2(b). For $\kappa > \kappa_c$, as clearly seen in Fig. 2(c), the original point becomes a saddle point and two degenerate minimum points appear at $[0, \pm\sqrt{(3\kappa - 1)/\kappa}]$.

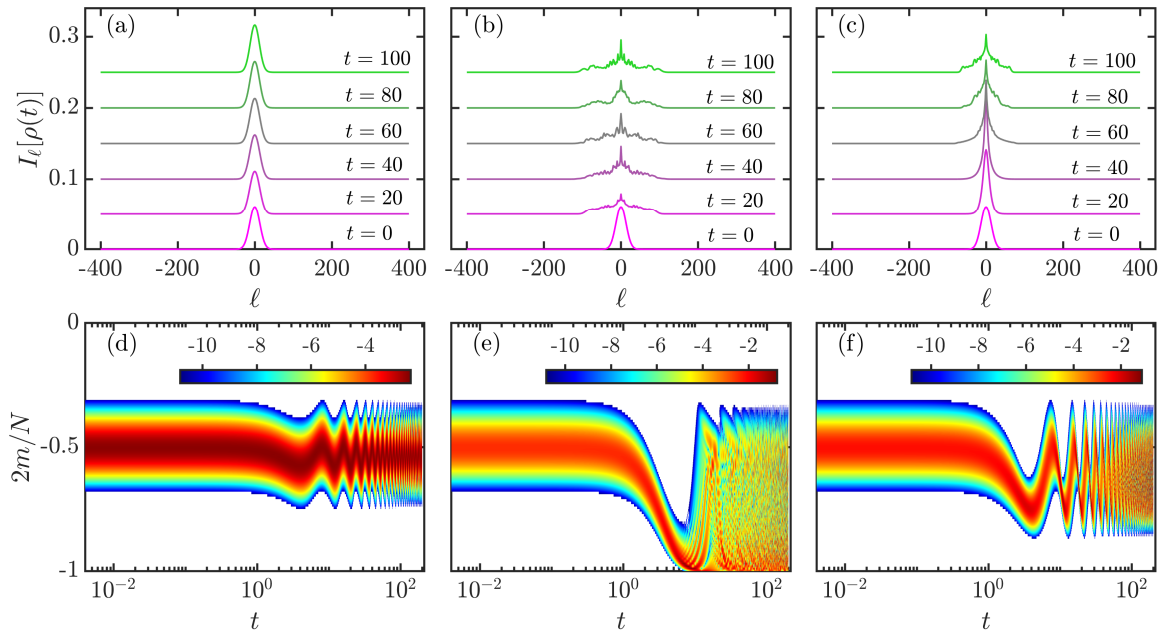


FIG. 3. Panels (a)-(c): Evolved MQC spectrum $\{I_\ell[\rho(t)]\}_{\ell=-2j}^{\ell=2j}$ of the LMG model at $\chi = 0.2\chi_\kappa^c$ (a), $\chi = \chi_\kappa^c$ (b), and $\chi = 2\chi_\kappa^c$ (c) for several times t in steps $\Delta t = 20$. The spectrum at fixed t has been shifted along y direction by $0.0025t$ in order to offer a three-dimensional-like visualization. Panels (d)-(f): Hot map plot displaying $\ln[|\zeta_m(t)|^2]$ as a function of m and t for the same values of χ as in panels (a)-(c). White color represents $|\zeta_m(t)|^2 = 0$. Other parameters: $N = 2j = 400$, $\kappa = 1.5\kappa_c$ and $\kappa_c = 1/3$. The axes in all panels are dimensionless.

The variation of energy surface implies an abrupt change in the nature of the available phase space volume for a certain energy E , which defined as

$$\rho_{cl}(E) = \frac{1}{(2\pi)^f} \iint \delta[E - \mathcal{H}_c(p, q)] dpdq, \quad (11)$$

where f denotes the degrees of freedom of the system, for the LMG model, we have $f = 1$. Notice that $\rho_{cl}(E)$ is the lowest-order term in the Gutzwiller trace formula [114] and identified as the classical approximation of the quantum density of states [3, 11, 12].

Following the approach outlined in Refs. [11, 12], we evaluate $\rho_{cl}(E)$ for two different values of κ and plot the results in the insets of Fig. 1. One can see that $\rho_{cl}(E)$ shows an excellent agreement with numerical results. Moreover, as expected, the behavior of $\rho_{cl}(E)$ undergoes a remarkable change as κ passes through its critical value. For $\kappa > \kappa_c$, the ESQPT at $E_c = 0$ is clearly signaled by the presence of the cusp-type singularity in $\rho_{cl}(E)$. In fact, due to the separatrix of the classical dynamics at the saddle point of $\mathcal{H}_c(p, q)$ [see Fig. 2(c)], $\rho_{cl}(E)$ exhibits a logarithmic divergence around E_c [3, 11], consistent with the divergent behavior of $\rho(E)$. This means the emergence of ESQPT in the LMG model can be recognized as a consequence of the saddle point in the corresponding classical dynamics.

IV. RESULTS

To demonstrate the usefulness of the MQC spectrum for studying of ESQPT in the LMG model, we consider the following sudden quench protocol. Initially, the system is prepared in the ground state, $|\psi_0\rangle$, of $H_0 = H$ with $\kappa_c < \kappa < 1$. At $t = 0$, an interaction with strength χ is suddenly added; then we investigate the evolution of the system under the postquench Hamiltonian $H_1 = H - (2\chi/N)J_x^2$.

The sudden quench process results in the dependence of the system energy on χ , which allows us to take the system through different ESQPT phases by varying the value of χ . As a consequence, we identify the value of χ that makes the system energy equals to the critical energy $E_c = 0$ as the critical quench strength χ_κ^c . The value of χ_κ^c can be obtained by means of the classical approach with the result given by

$$\chi_\kappa^c = -\frac{\kappa(3\kappa - 1)}{\kappa + 1}, \quad (12)$$

with $\kappa_c < \kappa < 1$.

With the aim to analyze the power of the MQC spectrum for characterizing ESQPT, we will first discuss the manifestations of ESQPT in the MQC spectrum of the evolved state. Subsequently, we show that the dynamical behaviors of the MQC spectrum width can be used to signal ESQPT. We finally investigate how to charac-

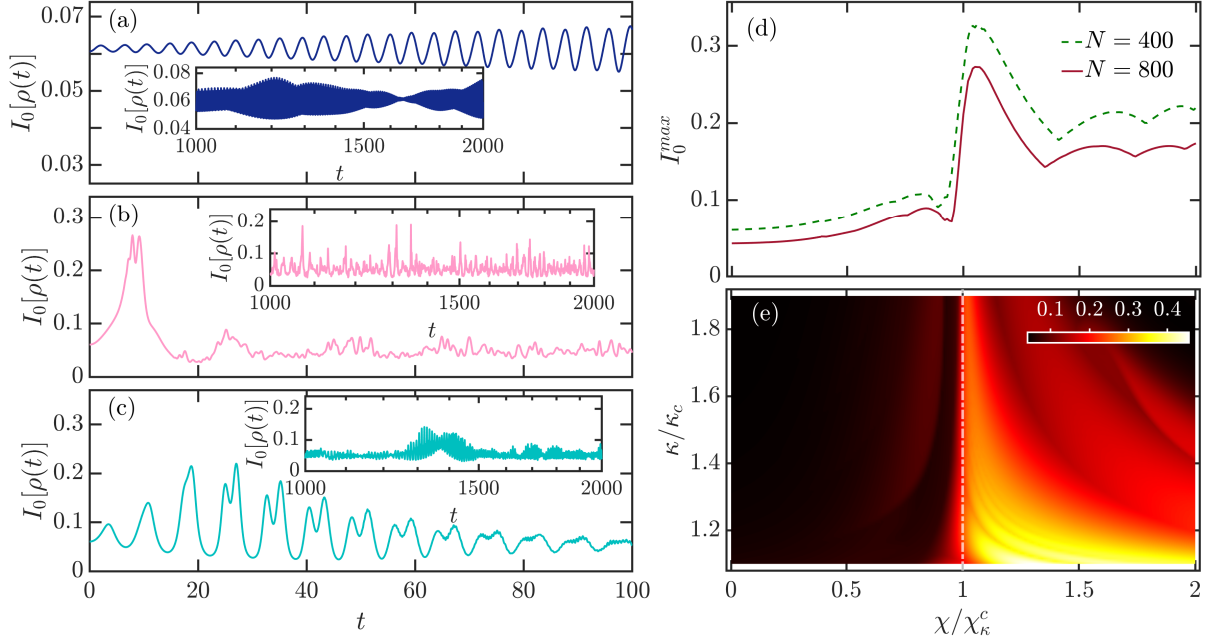


FIG. 4. Panels (a)-(c): $I_0[\rho(t)]$ (17) as a function of t for $\chi = 0.2\chi_c^c$ (a), $\chi = \chi_c^c$ (b), and $\chi = 2\chi_c^c$ (c) with $\kappa = 0.5$ and system size $N = 400$. The inset in each panel plots the time dependence of $I_0[\rho(t)]$ with $t \in [1000, 2000]$ for the corresponding values of χ . (d) I_0^{max} in Eq. (18) as a function of χ/χ_c^c for different system sizes with $\kappa = 0.5$. (e) I_0^{max} (18) as a function of χ/χ_c^c and κ/κ_c with system size $N = 800$. The vertical white dot-dashed line indicates the critical line $\chi = \chi_c^c$. The axes in all panels are dimensionless.

terize ESQPT using the MQC spectrum of the long time averaged state.

A. MQC spectrum of the evolved state

We start by calculating the MQC spectrum of the evolved state. The quantum state of the system at time t is given by

$$\rho(t) = |\psi_t\rangle\langle\psi_t| = e^{-iH_1 t} \rho(0) e^{iH_1 t}, \quad (13)$$

where $\rho(0) = |\psi_0\rangle\langle\psi_0|$ is the initial state of the system. To obtain the MQC spectrum of $\rho(t)$, we calculate the MQC intensities with respect to the collective spin operator J_z . Therefore, we decompose $\rho(t)$ in the eigenbasis of J_z , $\{|m\rangle\}_{m=-j}^{m=j}$, as follows

$$\rho(t) = \sum_{\ell} \rho_{\ell}(t), \quad (14)$$

where $\rho_{\ell}(t) = \sum_m \rho_{m+\ell, m}(t) |m+\ell\rangle\langle m|$ and

$$\begin{aligned} \rho_{m+\ell, m}(t) &= \langle m+\ell | \rho(t) | m \rangle \\ &= \langle m+\ell | e^{-iH_1 t} |\psi_0\rangle\langle\psi_0| e^{iH_1 t} | m \rangle \\ &= \zeta_{m+\ell}(t) \zeta_m^*(t), \end{aligned} \quad (15)$$

with $\zeta_s(t) = \langle s | \psi(t) \rangle = \sum_k \langle s | k \rangle \langle k | \psi_0 \rangle e^{-iE_k t}$. Here, $|k\rangle$ be the eigenstates of the postquench Hamiltonian H_1 ,

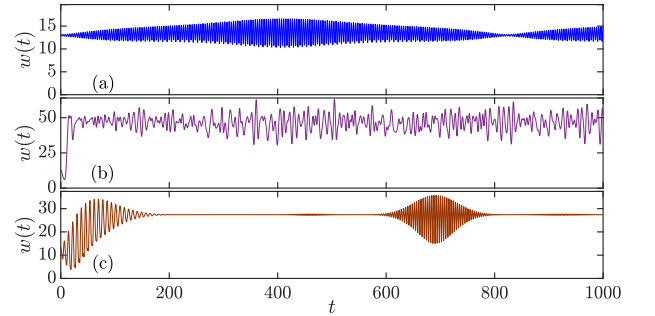


FIG. 5. Time evolution of $w(t)$ in Eq. (19) for $\chi/\chi_c^c = 0.2$ (a), $\chi/\chi_c^c = 1$ (b), and $\chi/\chi_c^c = 2$ (c) with $\kappa = 0.5$ and system size $N = 400$. The axes in all figures are dimensionless.

such that $H_1 |k\rangle = E_k |k\rangle$. From the MQC intensity definition in Eq. (3), the ℓ th MQC intensity of $\rho(t)$ is given by

$$I_{\ell}[\rho(t)] = \text{Tr}[\rho_{\ell}^{\dagger}(t) \rho_{\ell}(t)] = \sum_m |\zeta_m(t)|^2 |\zeta_{m+\ell}(t)|^2. \quad (16)$$

Obviously, the time dependence of $|\zeta_m(t)|^2$ determines the behavior of the MQC spectrum $\{I_{\ell}[\rho(t)]\}_{\ell=-2j}^{\ell=2j}$.

Fig. 3 shows MQC spectrum of $\rho(t)$ and the corresponding $|\zeta_m(t)|^2$ for χ below, at and above its critical value, χ_c^c , with $\kappa = 0.5$ and $N = 400$. We observe that the evolution of the MQC spectrum has been

strongly effected by the underlying ESQPT. Specifically, the evolved MQC spectrum changes from a simple form for $\chi < \chi_\kappa^c$ case to a form with complex oscillations when $\chi \geq \chi_\kappa^c$. In particular, the distinct behavior of the MQC spectrum at $\chi = \chi_\kappa^c$ allows us to use it as a probe of ESQPT.

Different features exhibited in the evolution of the MQC spectrum stem from the variation of $|\zeta_m(t)|^2$ behaviors as the system passes through ESQPT. As illustrated in Fig. 3(d), for $\chi < \chi_\kappa^c$, $|\zeta_m(t)|^2$ oscillate regularly with respect to t , which gives rise to simple structures of the MQC spectrum. Once the critical point $\chi = \chi_\kappa^c$ is approached, the evolutions of $|\zeta_m(t)|^2$ are governed by irregular oscillations with tiny amplitude, as seen in Fig. 3(e). This leads to the complexity in the evolved MQC spectrum. Above the critical point, such as $\chi = 2\chi_\kappa^c$ case plotted in Fig. 3(f), we see that the regular oscillations in $|\zeta_m(t)|^2$ at initial time are followed by the random oscillations at larger time. This explains the structure transformation behavior observed in the evolved MQC spectrum [see Fig. 3(d)]. Furthermore, Fig. 3(e) suggests that there are a larger number of m contributing to $|\zeta_m(t)|^2$ at $\chi = \chi_\kappa^c$ compared to the cases with χ far away from χ_κ^c as long as $t \gtrsim 50$. This means that the evolved MQC spectrum would has maximal extension around the critical point after enough long time. This is in according with the results demonstrated in Figs. 3(a)-3(c).

In addition to the MQC spectrum, its individual component also acts as a useful detector of quantum phase transitions in various many-body quantum systems [65, 66]. Hence, to verify the MQC spectrum can signal ESQPT, we need further to investigate the interplay between ESQPT and an individual $I_\ell[\rho(t)]$.

Among $I_\ell[\rho(t)]$, we focus on an experimentally accessible quantity, $I_0[\rho(t)]$, which corresponds to the maximal MQC intensity and has following expression

$$I_0[\rho(t)] = \sum_m |\zeta_m(t)|^4. \quad (17)$$

Because of $\zeta_m(t) = \langle m|\psi(t)\rangle$, $I_0[\rho(t)]$ can be considered as the participation ratio [115–117], indicating that it measures the degree of delocalization of the evolved state $|\psi(t)\rangle$ in $\{|m\rangle\}_{m=-j}^{m=j}$ basis.

Figs. 4(a)-4(b) plot the evolution of $I_0[\rho(t)]$ for three different values of χ with $\kappa = 0.5$ and $N = 400$. Clearly, in contrast to the periodic oscillation with small amplitude exhibited in $\chi < \chi_\kappa^c$ phase [see Fig. 4(a)], the regular behavior in $I_0[\rho(t)]$ evolution quickly turns into an irregular pattern for $\chi > \chi_\kappa^c$ phase, as observed from Fig. 4(c). At the critical point $\chi = \chi_\kappa^c$, as can be seen from Fig. 4(b), $I_0[\rho(t)]$ undergoes a fast growth which rapidly decreases to a small value with random fluctuations. Therefore, both the phases and the existence of ESQPT can be identified through the dynamical properties of $I_0[\rho(t)]$.

To further demonstrate that $I_0[\rho(t)]$ behaves as a probe of ESQPT, we consider its maximum value, denoted by

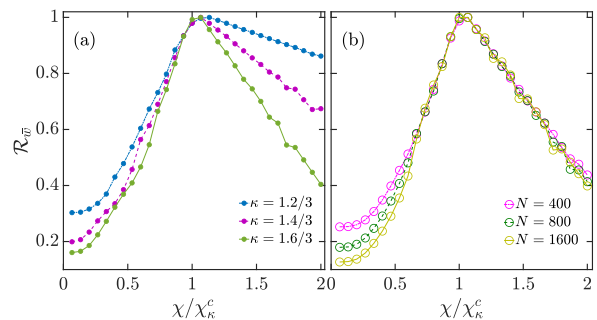


FIG. 6. The rescaled long time averaged width, $\mathcal{R}_{\bar{w}}$, as a function of χ/χ_κ^c for (a) several values of κ with $N = 1000$ and (b) different system sizes N with $\kappa = 1.6/3$. In both panels \bar{w} has been rescaled by its maximal value \bar{w}_m , so that $\mathcal{R}_{\bar{w}} = \bar{w}/\bar{w}_m$. The axes in all figures are dimensionless.

I_0^{max} , in a time interval $[0, \tau]$ and defined as

$$I_0^{max} = \max_{t \in [0, \tau]} \{I_0[\rho(t)]\}, \quad (18)$$

where the time length τ should be larger than the initial timescale. In our calculation, we set $\tau = 30$. A careful check on the cases with $\tau > 30$ shows that the present conclusions are still hold.

In Fig. 4(d), we plot the variation of I_0^{max} with χ/χ_κ^c for different system sizes with $\kappa = 0.5$. We clearly see that I_0^{max} undergoes an abrupt change in the neighborhood of the critical point, irrespective of the system size N . As a consequence, one can utilize I_0^{max} to unveil the underlying ESQPT in many-body quantum systems. This is further confirmed by the result shown in Fig. 4(e), where the phase boundary revealed by I_0^{max} is in good agreement with the analytical result.

B. The MQC spectrum width

The extension of the MQC spectrum with increasing χ/χ_κ^c , as observed in Figs. 3(a)-3(b), suggests that analyzing the width of the MQC spectrum would lead us to get more characters of ESQPT. In fact, it has been demonstrated that the MQC spectrum width plays an important role in the studies of quantum phase transitions for both Hermitian and non-Hermitian systems. In our work, we concerning its ability as a signature of ESQPT.

As MQC spectrum distributed symmetrically around $\ell = 0$, its width is given by the second moment in Eq. (4) with $\mathcal{O} = J_z$,

$$w(t) = \Sigma[\rho(t), J_z] = \sqrt{\sum_\ell \ell^2 I_\ell^{J_z}[\rho(t)]}. \quad (19)$$

In the following, we will show that both qualitative and quantitative features of $w(t)$ can be used to diagnose ESQPT.

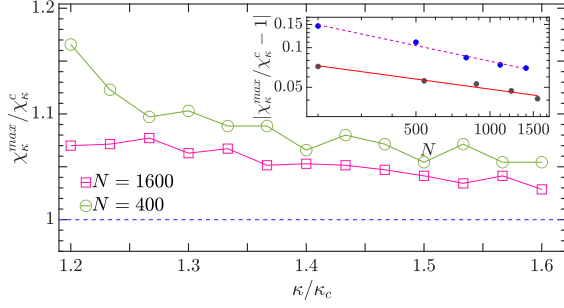


FIG. 7. The rescaled locations of the maximal \bar{w} , $\chi_\kappa^{max}/\chi_\kappa^c$, as a function of κ/κ_c for several values of system size N . The horizontal dashed line denotes $\chi_\kappa^{max}/\chi_\kappa^c = 1$. The inset shows $|\chi_\kappa^{max}/\chi_\kappa^c - 1|$ as a function of N (on a log-log scale) for $\kappa_1 = 1.3/3$ (blue dots) and $\kappa_1 = 0.5$ (gray dots). The purple dashed and red solid lines are of the form $|\chi_\kappa^{max}/\chi_\kappa^c - 1| = C_\kappa N^{-\beta_\kappa}$, with $C_{\kappa_1} = 1.2095$, $\beta_{\kappa_1} = 0.3952$ and $C_{\kappa_2} = 0.2801$, $\beta_{\kappa_2} = 0.2540$. The axes in all figures are dimensionless.

Let us first consider the signatures of ESQPT in the dynamics of $w(t)$. Fig. 5 shows the time evolution of $w(t)$ for different χ/χ_κ^c values. The effect of ESQPT on quantum coherence is clearly reflected in the evolutions of $w(t)$. One can see that, $w(t)$ has different behaviors in different phases of ESQPT, as illustrated in Figs. 5(a) and 5(c), respectively. This enables us to distinguish the different phases of ESQPT via the dynamical features of $w(t)$. Importantly, the singular time dependence of $w(t)$ particular at the critical point [see Fig. 5(b)] implies $w(t)$ is a useful ESQPT witness.

To further illustrate $w(t)$ acts as a diagnostic tool for probing ESQPT, we consider the long time averaged width, defined as

$$\bar{w} = \lim_{T \rightarrow \infty} \frac{1}{T} \int_{t_0}^{t_0+T} w(t) dt. \quad (20)$$

It quantifies the time average of $w(t)$ between $t_0 \leq t \leq T$ with $t_0 \gg 1$. In our simulation, we choose $t_0 = 10^4$ and $T = 10^3$. A carefully check demonstrates that the present results are not modified for more larger t_0 and T values.

From the results in Fig. 5, one can expect that \bar{w} should reach its maximal value around the critical point of ESQPT. This is evident in Fig. 6, where we plot \bar{w} , as a function of χ/χ_κ^c for different κ with fixed N and for several N with fixed κ , respectively. One can clearly see that \bar{w} has a peak around $\chi/\chi_\kappa^c = 1$, regardless of the strength of the control parameter κ and the system size N . This means that the peak in \bar{w} acts as the precursor of ESQPT and the location of the peak can be identified

as the numerical estimation of the critical χ value. Moreover, the peak tends towards $\chi/\chi_\kappa^c = 1$ with increasing system size N . Therefore, the larger the system size N , the higher the estimate accuracy of the critical point of ESQPT.

The aforementioned results are confirmed in Fig. 7, where the locations of the maximal \bar{w} , denoted by χ_κ^{max} , at several values of κ have been plotted for different system sizes N . To quantitatively analyze how χ_κ^{max} tends to χ_κ^c as N increases, we include the inset in Fig. 7, where the variation of $|\chi_\kappa^{max}/\chi_\kappa^c - 1|$ with the system size N for $\kappa = 1.3/3$ and $\kappa = 0.5$ have been plotted on a log-log scale. We see that, regardless of the κ value, the scaling behavior of $|\chi_\kappa^{max}/\chi_\kappa^c - 1|$ is well fitted by a power law, $|\chi_\kappa^{max}/\chi_\kappa^c - 1| = C_\kappa N^{-\beta_\kappa}$, with C_κ and β_κ are κ dependent quantities. Hence, we have $\chi_\kappa^{max} \rightarrow \chi_\kappa^c$ as N goes to infinite.

C. MQC spectrum of the long time averaged state

We now discuss how to unveil the signatures of ESQPT through the MQC spectrum of the long time averaged state, which defined as

$$\begin{aligned} \bar{\rho} &= \lim_{T \rightarrow \infty} \frac{1}{T} \int_0^T dt \rho(t) \\ &= \lim_{T \rightarrow \infty} \frac{1}{T} \int_0^T dt e^{-iH_1 t} |\psi_0\rangle \langle \psi_0| e^{iH_1 t}. \end{aligned} \quad (21)$$

To calculate the MQC spectrum of $\bar{\rho}$, we first expand it in $\{|m\rangle\}_{m=-j}^{m=j}$ basis as

$$\bar{\rho} = \sum_\ell \bar{\rho}_\ell, \quad (22)$$

where

$$\bar{\rho}_\ell = \sum_m \bar{\rho}_{m+\ell, m} |m+\ell\rangle \langle m|, \quad (23)$$

with

$$\begin{aligned} \bar{\rho}_{m+\ell, m} &= \langle m+\ell | \bar{\rho} | m \rangle \\ &= \lim_{T \rightarrow \infty} \frac{1}{T} \int_0^T \langle m+\ell | e^{-iH_1 t} |\psi_0\rangle \langle \psi_0| e^{iH_1 t} | m \rangle. \end{aligned} \quad (24)$$

Then, by inserting the identity operator $\mathbf{1} = \sum_k |k\rangle \langle k|$ with $|k\rangle$ being the k th eigenstate of the postquench Hamiltonian H_1 , one arrives at

$$\bar{\rho}_{m+\ell, m} = \lim_{T \rightarrow \infty} \frac{1}{T} \int_0^T \sum_{k, k'} \langle m+\ell | k \rangle \langle k | \psi_0 \rangle \langle \psi_0 | k' \rangle \langle k' | m \rangle e^{-i(E_k - E_{k'})t} = \sum_k \langle m+\ell | k \rangle \langle k | m \rangle |\langle \psi_0 | k \rangle|^2 = \mathcal{D}_{m+\ell, m}, \quad (25)$$

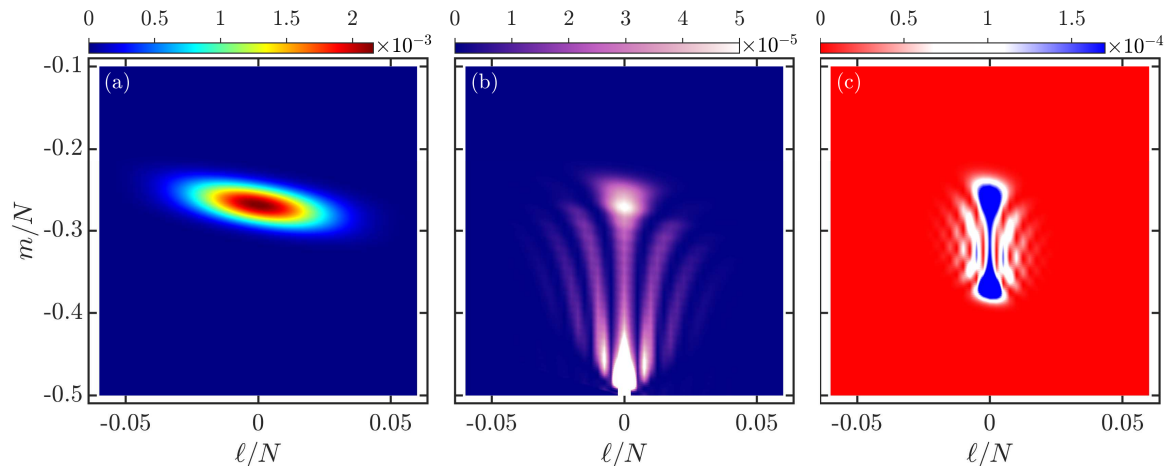


FIG. 8. $\mathcal{D}_{m+l,m}$ in Eq. (25) as a function of ℓ/N and m/N for (a) $\chi/\chi_\kappa^c = 0.2$, (b) $\chi/\chi_\kappa^c = 1$, and (c) $\chi/\chi_\kappa^c = 2$ with $\kappa = 0.5$ and $N = 800$. The axes in all figures are dimensionless.

where $E_k(E_{k'})$ is the eigenenergy of the k th (k' th) eigenstate and the intergration has been carried out by noting the fact that there is no degeneracy in the energy spectrum of the postquench Hamiltonian H_1 . Finally, the resulting ℓ th component of MQC spectrum is

$$I_\ell(\bar{\rho}) = \text{Tr}[\bar{\rho}_\ell^\dagger \bar{\rho}_\ell] = \sum_m |\mathcal{D}_{m+l,m}|^2. \quad (26)$$

The formula indicates that the MQC spectrum of $\bar{\rho}$ is determined by the dependence of $\mathcal{D}_{m+l,m}$ on ℓ and m .

Fig. 8 plots $\mathcal{D}_{m+l,m}$ as a function of m and ℓ for different values of χ/χ_κ^c with $\kappa = 0.5$. We see an obvious variation in the behavior of $\mathcal{D}_{m+l,m}$ as the system passes through the ESQPT. Specifically, $\mathcal{D}_{m+l,m}$ behaves as a smooth function in the phase with $\chi/\chi_\kappa^c < 1$ and has a wide range of support along ℓ direction, as evident from Fig. 8(a). On the contrary, in the phase of $\chi/\chi_\kappa^c > 1$ [see Fig. 8(c)], $\mathcal{D}_{m+l,m}$ shows a complex pattern and quickly decays to zero as $|\ell|$ increases. At the critical point $\chi/\chi_\kappa^c = 1$, as illustrated in Fig. 8(b), $\mathcal{D}_{m+l,m}$ displays a remarkable different behavior. Although it also exhibits a complex pattern, the range of its support along both m and ℓ directions are wide. In particular, $\mathcal{D}_{m+l,m}$ has the minimal value at the critical point of ESQPT.

The observed features of $\mathcal{D}_{m+l,m}$ in Fig. 8 suggest that the underlying ESQPT will lead to a specific and notable change in the MQC spectrum. This is indeed what we seen in Fig. 9(a), where we depict MQC spectrum as a function of χ/χ_κ^c for the case with $\kappa = 0.5$. As the range of support along ℓ direction in $\mathcal{D}_{m+l,m}$ exhibits a rapid decrease as χ passes through its critical value, the MQC spectrum undergoes a sharp change as χ increases. Moreover, the higher values of $\mathcal{D}_{m+l,m}$ for $\chi/\chi_\kappa^c < 1$ case [compare the color bar scale in Fig. 8(a) with Figs. 8(b) and 8(c)] further signify the larger amplitudes of the MQC spectrum in the corresponding phase. These features are

more visible in Fig. 9(b), where the MQC spectrum for several χ/χ_κ^c values are plotted.

The results in Figs. 9(a) and 9(b) confirm that the MQC spectrum of $\bar{\rho}$ acts as an indicator for witnessing the ESQPT in many-body quantum system. To further demonstrate the usefulness of the MQC distribution of $\bar{\rho}$ in the studies of ESQPT, let us now focus on the zero mode in $\{I_\ell(\bar{\rho})\}_{\ell=-2j}^{\ell=2j}$, denoted as $I_0(\bar{\rho})$ and calculated by

$$I_0(\bar{\rho}) = \sum_m |\mathcal{D}_{m,m}|^2, \quad (27)$$

where $\mathcal{D}_{m,m} = \sum_k |\langle m|k\rangle|^2 |\langle \psi_0|k\rangle|^2$.

Fig. 9(c) shows the evolution of $I_0(\bar{\rho})$ as a function of κ and χ . Overall, we see that the value of $I_0(\bar{\rho})$ in $\chi/\chi_\kappa^c < 1$ phase is larger than that of $\chi/\chi_\kappa^c > 1$ phase. This is due to the values of $\mathcal{D}_{m,m}$ is much larger in the phase of $\chi/\chi_\kappa^c < 1$, as shown in Figs. 8(a) and 8(c). A prominent feature exhibited in Fig. 9(c) is that $I_0(\bar{\rho})$ has a peak around the critical point, regardless of the value of κ . This is more evident from Fig. 9(d) where the dependence of $I_0(\bar{\rho})$ on χ/χ_κ^c for several κ values have been plotted. The peak shown in $I_0(\bar{\rho})$ can trace back to the wider range of support along m direction in $\mathcal{D}_{m,m}$, as seen in Fig. 8(b). Hence, the ESQPT can also be probed by the zero mode of the MQC spectrum of $\bar{\rho}$.

Furthermore, as MQC spectrum has different width in two phases of ESQPT, one would expect that the width of the MQC spectrum of $\bar{\rho}$ should also be able to diagnose the presence of ESQPT. To verify this, we show how the rescaled width, $\tilde{w}(\bar{\rho}) = w(\bar{\rho})/N$, of the MQC spectrum of $\bar{\rho}$ evolves as a function of κ and χ in Fig. 9(e). We see that \tilde{w} has a valley at the critical point, regardless of the value of κ , in contrast to the case of long time averaged $w(t)$ which exhibits a high peak in the neighborhood of the critical point, as seen in Fig. 6. The valley in the behavior of $\tilde{w}(\bar{\rho})$

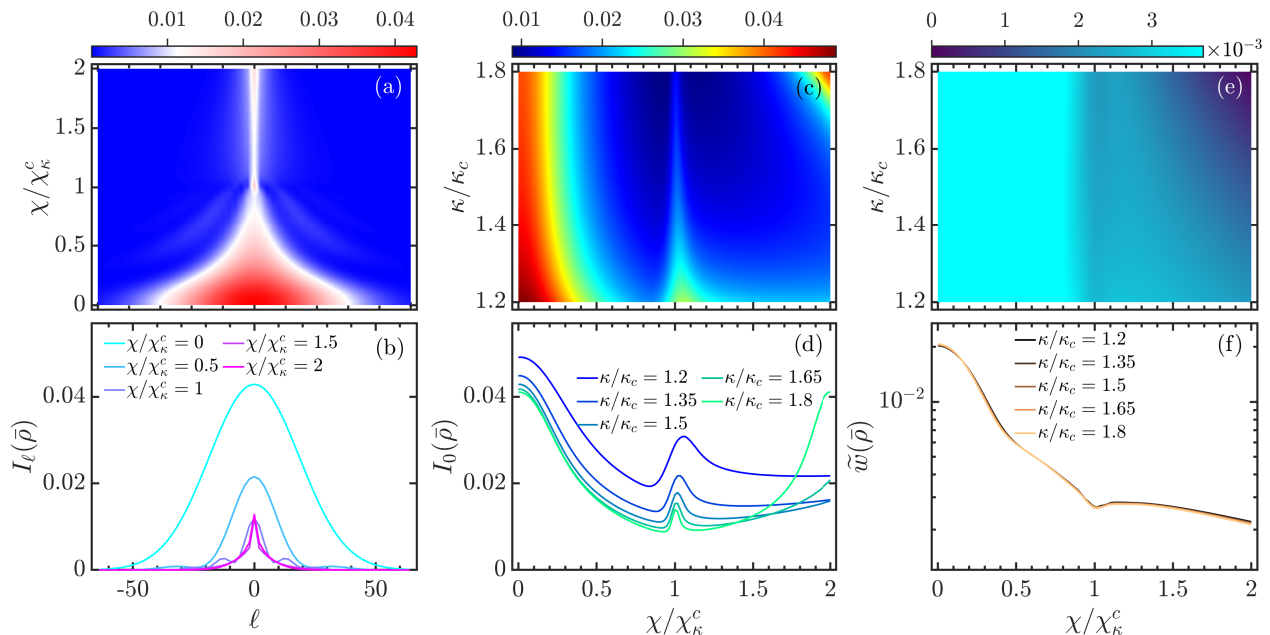


FIG. 9. (a) Heat map depicting MQC spectrum $\{I_\ell(\bar{\rho})\}_{\ell=-2j}^{\ell=2j}$ as a function of ℓ and χ/χ_κ^c for $\kappa = 0.5$. (b) $I_\ell(\bar{\rho})$ as a function of ℓ for several values of χ/χ_κ^c with $\kappa = 0.5$. (c) $I_0(\bar{\rho})$ (27) as a function of χ/χ_κ^c and κ/κ_c . (d) $I_0(\bar{\rho})$ as a function of χ/χ_κ^c for different values of κ/κ_c . (e) The rescaled width of the MQC spectrum $\{I_\ell(\bar{\rho})\}_{\ell=-2j}^{\ell=2j}$, $\tilde{w}(\bar{\rho}) = w(\bar{\rho})/N$, as a function of χ/χ_κ^c and κ/κ_c . (f) $\tilde{w}(\bar{\rho})$ as a function of χ/χ_κ^c for several values of κ/κ_c . Other parameters: $N = 2j = 800$ and $\kappa_c = 1/3$. The axes in all figures are dimensionless.

can be more clearly observed in Fig. 9(f), where $\tilde{w}(\bar{\rho})$ as a function of χ/χ_κ^c with increasing κ has been plotted. This visible valley in $\tilde{w}(\bar{\rho})$ is a consequence of the lowest $\mathcal{D}_{m+\ell,m}$ value at the critical point [cf. Fig. 8(b)]. We finally note that the evolution of $\tilde{w}(\bar{\rho})$ as a function of χ/χ_κ^c is almost independent of κ .

V. CONCLUSION

In this work we have investigated interplay of ESQPT and the signatures of quantum coherence in the LMG model by means of the MQC spectrum. We have shown how to identify the characters of ESQPT in various properties of the MQC spectrum.

The ESQPT in the LMG model is signified by the logarithmic divergence of the density of states at the critical energy. To understand this divergence behavior, we have performed a detailed analysis on the classical counterpart of the system and unveiled that the divergence behavior in the density of states correlates with the saddle point in the classical Hamiltonian.

By using the sudden quench protocol and expanding the evolved state in the chosen basis, we have found that the underlying ESQPT has strong impact on the time evolution of the MQC spectrum. The particular evolution behavior of the MQC spectrum at the critical point serves as a reliable indicator to probe the presence of

ESQPT. We further demonstrated that the emergence of ESQPT can be well captured by the zero mode and the width of the MQC spectrum. In particular, we shown that the long time averaged width of the MQC spectrum exhibits a peak near the critical point of ESQPT. In addition, the location of the peak tends to the critical point with increasing system size. We also carried out an explicit analysis on the properties of the MQC distribution of the long time averaged state, which defined as the long time average of the evolved state [cf. Eq. (21)]. We have seen that the ESQPT can be witnessed by an abrupt change in the behavior of the MQC spectrum of the long time averaged state. Moreover, its zero mode and width also stand as good detector for witnessing the ESQPT in the quantum many-body system.

Finally, we would like to point out that the LMG model has been realized in a wide variety of experimental platforms, such as trapped ions [63, 106, 118], cold atoms [107], Bose-Einstein condensates [104, 105] and superconducting simulator [108]. On the other hand, the experimental measurement of the MQC spectrum has been either achieved in [63] or proposed in [65]. Hence, we expect that our results would motivate further experimental efforts to investigate ESQPT using the MQC spectrum.

ACKNOWLEDGMENTS

Q. W. acknowledges support from the National Science Foundation of China under Grant No. 11805165, Zhejiang Provincial Nature Science Foundation under Grant No. LY20A050001, and the Slovenian Research Agency (ARRS) under the Grant No. J1-9112. This work has also been partially supported by the Consejería de Conocimiento, Investigación y Universidad,

Junta de Andalucía and European Regional Development Fund (ERDF), ref. SOMM17/6105/UGR and by the Ministerio de Ciencia, Innovación y Universidades (ref.COOPB20364). FPB also thanks support from project UHU-1262561. Computing resources supporting this work were partly provided by the CEAFCM and Universidad de Huelva High Performance Computer (HPC@UHU) located in the Campus Universitario el Carmen and funded by FEDER/MINECO project UNHU-15CE-2848.

-
- [1] S. Sachdev, *Physics World* **12**, 33 (1999).
- [2] L. Carr, *Understanding quantum phase transitions* (CRC press, 2010).
- [3] M. Caprio, P. Cejnar, and F. Iachello, *Ann. Phys. (NY)* **323**, 1106 (2008).
- [4] A. L. Corps and A. Relaño, *Phys. Rev. Lett.* **127**, 130602 (2021).
- [5] P. Cejnar, P. Stránský, M. Macek, and M. Kloc, *J. Phys. A: Math. Theor.* **54**, 133001 (2021).
- [6] P. Stránský, M. Macek, and P. Cejnar, *Ann. Phys.* **345**, 73 (2014).
- [7] F. Leyvraz and W. D. Heiss, *Phys. Rev. Lett.* **95**, 050402 (2005).
- [8] M. Šindelka, L. F. Santos, and N. Moiseyev, *Phys. Rev. A* **95**, 010103 (2017).
- [9] L. F. Santos and F. Pérez-Bernal, *Phys. Rev. A* **92**, 050101 (2015).
- [10] L. F. Santos, M. Távora, and F. Pérez-Bernal, *Phys. Rev. A* **94**, 012113 (2016).
- [11] D. J. Nader, C. A. González-Rodríguez, and S. Lerma-Hernández, *Phys. Rev. E* **104**, 064116 (2021).
- [12] M. A. Bastarrachea-Magnani, S. Lerma-Hernández, and J. G. Hirsch, *Phys. Rev. A* **89**, 032101 (2014).
- [13] P. Pérez-Fernández, P. Cejnar, J. M. Arias, J. Dukelsky, J. E. García-Ramos, and A. Relaño, *Phys. Rev. A* **83**, 033802 (2011).
- [14] T. Brandes, *Phys. Rev. E* **88**, 032133 (2013).
- [15] R. Puebla, M.-J. Hwang, and M. B. Plenio, *Phys. Rev. A* **94**, 023835 (2016).
- [16] P. Feldmann, C. Klempt, A. Smerzi, L. Santos, and M. Gessner, *Phys. Rev. Lett.* **126**, 230602 (2021).
- [17] J. Cabedo and A. Celi, *Phys. Rev. Research* **3**, 043215 (2021).
- [18] D. Larese, F. Pérez-Bernal, and F. Iachello, *J. Mol. Struct.* **1051**, 310 (2013).
- [19] J. Khalouf-Rivera, F. Pérez-Bernal, and M. Carvajal, *J. Quant. Spectrosc. Radiat. Transfer* **261**, 107436 (2021).
- [20] J. Khalouf-Rivera, M. Carvajal, and F. Pérez-Bernal, *SciPost Phys.* **12**, 2 (2022).
- [21] V. M. Bastidas, P. Pérez-Fernández, M. Vogl, and T. Brandes, *Phys. Rev. Lett.* **112**, 140408 (2014).
- [22] I. García-Mata, E. Vergini, and D. A. Wisniacki, *Phys. Rev. E* **104**, L062202 (2021).
- [23] M. Macek, P. Stránský, A. Leviatan, and P. Cejnar, *Phys. Rev. C* **99**, 064323 (2019).
- [24] W.-T. Dong, Y. Zhang, B.-C. He, F. Pan, Y.-A. Luo, J. P. Draayer, and S. Karampagia, *J. Phys. G: Nucl. Part. Phys.* **48**, 045103 (2021).
- [25] Q. Wang and F. Pérez-Bernal, *Phys. Rev. E* **104**, 034119 (2021).
- [26] D. Mondal, S. Sinha, and S. Sinha, *Phys. Rev. E* **105**, 014130 (2022).
- [27] Q.-W. Wang and S. Wu, *Phys. Rev. A* **102**, 063531 (2020).
- [28] B. Dietz, F. Iachello, M. Miski-Oglu, N. Pietralla, A. Richter, L. von Smekal, and J. Wambach, *Phys. Rev. B* **88**, 104101 (2013).
- [29] F. Iachello, B. Dietz, M. Miski-Oglu, and A. Richter, *Phys. Rev. B* **91**, 214307 (2015).
- [30] T. Tian, H.-X. Yang, L.-Y. Qiu, H.-Y. Liang, Y.-B. Yang, Y. Xu, and L.-M. Duan, *Phys. Rev. Lett.* **124**, 043001 (2020).
- [31] J. Gamito, J. Khalouf-Rivera, J. M. Arias, P. Pérez-Fernández, and F. Pérez-Bernal, (2022), [arXiv:2202.11413 \[quant-ph\]](https://arxiv.org/abs/2202.11413).
- [32] A. Relaño, J. M. Arias, J. Dukelsky, J. E. García-Ramos, and P. Pérez-Fernández, *Phys. Rev. A* **78**, 060102 (2008).
- [33] P. Pérez-Fernández, A. Relaño, J. M. Arias, J. Dukelsky, and J. E. García-Ramos, *Phys. Rev. A* **80**, 032111 (2009).
- [34] Q. Wang and F. Pérez-Bernal, *Phys. Rev. A* **100**, 022118 (2019).
- [35] R. Puebla, A. Relaño, and J. Retamosa, *Phys. Rev. A* **87**, 023819 (2013).
- [36] R. Puebla and A. Relaño, *Phys. Rev. E* **92**, 012101 (2015).
- [37] Z.-G. Yuan, P. Zhang, S.-S. Li, J. Jing, and L.-B. Kong, *Phys. Rev. A* **85**, 044102 (2012).
- [38] G. Engelhardt, V. M. Bastidas, W. Kopylov, and T. Brandes, *Phys. Rev. A* **91**, 013631 (2015).
- [39] Q. Wang and H. T. Quan, *Phys. Rev. E* **96**, 032142 (2017).
- [40] P. Cejnar and P. Stránský, *Phys. Lett. A* **381**, 984 (2017).
- [41] P. Pérez-Fernández and A. Relaño, *Phys. Rev. E* **96**, 012121 (2017).
- [42] M. Kloc, P. Stránský, and P. Cejnar, *Ann. Phys.* **382**, 85 (2017).
- [43] M. Kloc, P. Stránský, and P. Cejnar, *Phys. Rev. A* **98**, 013836 (2018).
- [44] Q. Hummel, B. Geiger, J. D. Urbina, and K. Richter, *Phys. Rev. Lett.* **123**, 160401 (2019).
- [45] Q. Wang and F. Pérez-Bernal, *Phys. Rev. A* **100**, 062113 (2019).

- [46] Z. Mzaouali, R. Puebla, J. Gould, M. El Baz, and S. Campbell, *Phys. Rev. E* **103**, 032145 (2021).
- [47] Q. Wang and F. Pérez-Bernal, *Phys. Rev. E* **103**, 032109 (2021).
- [48] P. Stránský, P. Cejnar, and R. Filip, *Phys. Rev. A* **104**, 053722 (2021).
- [49] M. Kloc, D. Šimsa, F. Hanák, P. R. Kaprálová-Ždánková, P. Stránský, and P. Cejnar, *Phys. Rev. A* **103**, 032213 (2021).
- [50] J. Khalouf-Rivera, F. Pérez-Bernal, and M. Carvajal, *Phys. Rev. A* **105**, 032215 (2022).
- [51] C. M. Lóbez and A. Relaño, *Phys. Rev. E* **94**, 012140 (2016).
- [52] P. Pérez-Fernández, A. Relaño, J. M. Arias, P. Cejnar, J. Dukelsky, and J. E. García-Ramos, *Phys. Rev. E* **83**, 046208 (2011).
- [53] Á. L. Corps, R. A. Molina, and A. Relaño, *J. Phys. A: Math. Theor.* **55**, 084001 (2022).
- [54] S. P. Kelly, E. Timmermans, and S.-W. Tsai, *Phys. Rev. A* **102**, 052210 (2020).
- [55] M. R. Lambert, S.-W. Tsai, and S. P. Kelly, *Phys. Rev. A* **106**, 012206 (2022).
- [56] A. Streltsov, G. Adesso, and M. B. Plenio, *Rev. Mod. Phys.* **89**, 041003 (2017).
- [57] J. Baum, M. Munowitz, A. N. Garroway, and A. Pines, *J. Chem. Phys.* **83**, 2015 (1985).
- [58] P. Cappellaro, “Implementation of state transfer hamiltonians in spin chains with magnetic resonance techniques,” in *Quantum State Transfer and Network Engineering*, edited by G. M. Nikolopoulos and I. Jex (Springer Berlin Heidelberg, Berlin, Heidelberg, 2014) pp. 183–222.
- [59] K. Macieszczak, E. Levi, T. Macrì, I. Lesanovsky, and J. P. Garrahan, *Phys. Rev. A* **99**, 052354 (2019).
- [60] S. I. Doronin, *Phys. Rev. A* **68**, 052306 (2003).
- [61] G. B. Furman, V. M. Meerovich, and V. L. Sokolovsky, *Phys. Rev. A* **78**, 042301 (2008).
- [62] E. B. Fel’dman, A. N. Pyrkov, and A. I. Zenchuk, *Phil. Trans. R. Soc. A* **370**, 4690 (2012).
- [63] M. Gärttner, J. G. Bohnet, A. Safavi-Naini, M. L. Wall, J. J. Bollinger, and A. M. Rey, *Nat. Phys.* **13**, 781 (2017).
- [64] M. Gärttner, P. Hauke, and A. M. Rey, *Phys. Rev. Lett.* **120**, 040402 (2018).
- [65] R. J. Lewis-Swan, S. R. Muleady, and A. M. Rey, *Phys. Rev. Lett.* **125**, 240605 (2020).
- [66] D. P. Pires and T. Macrì, *Phys. Rev. B* **104**, 155141 (2021).
- [67] M. Munowitz, A. Pines, and M. Mehring, *J. Chem. Phys.* **86**, 3172 (1987).
- [68] C. M. Sánchez, R. H. Acosta, P. R. Levstein, H. M. Pastawski, and A. K. Chattah, *Phys. Rev. A* **90**, 042122 (2014).
- [69] G. A. Álvarez and D. Suter, *Phys. Rev. Lett.* **104**, 230403 (2010).
- [70] G. A. Álvarez, D. Suter, and R. Kaiser, *Science* **349**, 846 (2015).
- [71] K. X. Wei, C. Ramanathan, and P. Cappellaro, *Phys. Rev. Lett.* **120**, 070501 (2018).
- [72] H. T. Quan, Z. Song, X. F. Liu, P. Zanardi, and C. P. Sun, *Phys. Rev. Lett.* **96**, 140604 (2006).
- [73] S.-J. GU, *Int. J. Mod. Phys. B* **24**, 4371 (2010).
- [74] H. Lipkin, N. Meshkov, and A. Glick, *Nucl. Phys.* **62**, 188 (1965).
- [75] I. Homrighausen, N. O. Abeling, V. Zauner-Stauber, and J. C. Halimeh, *Phys. Rev. B* **96**, 104436 (2017).
- [76] N. Defenu, T. Enss, M. Kastner, and G. Morigi, *Phys. Rev. Lett.* **121**, 240403 (2018).
- [77] J. Lang, B. Frank, and J. C. Halimeh, *Phys. Rev. Lett.* **121**, 130603 (2018).
- [78] J. Lang, B. Frank, and J. C. Halimeh, *Phys. Rev. B* **97**, 174401 (2018).
- [79] Á. L. Corps and A. Relaño, arXiv e-prints , arXiv:2205.03443 (2022), arXiv:2205.03443 [cond-mat.stat-mech].
- [80] R. Botet and R. Jullien, *Phys. Rev. B* **28**, 3955 (1983).
- [81] S. Dusuel and J. Vidal, *Phys. Rev. Lett.* **93**, 237204 (2004).
- [82] F. Leyvraz and W. D. Heiss, *Phys. Rev. Lett.* **95**, 050402 (2005).
- [83] P. Ribeiro, J. Vidal, and R. Mosseri, *Phys. Rev. Lett.* **99**, 050402 (2007).
- [84] P. Titum and M. F. Maghrebi, *Phys. Rev. Lett.* **125**, 040602 (2020).
- [85] S. Campbell, *Phys. Rev. B* **94**, 184403 (2016).
- [86] Y.-H. Ma, S.-H. Su, and C.-P. Sun, *Phys. Rev. E* **96**, 022143 (2017).
- [87] A. U. C. Hardal, M. Paternostro, and O. E. Müstecaplıođlu, *Phys. Rev. E* **97**, 042127 (2018).
- [88] Z.-Z. Zhang and W. Wu, arXiv e-prints , arXiv:2206.04422 (2022), arXiv:2206.04422 [quant-ph].
- [89] G. Salvatori, A. Mandarino, and M. G. A. Paris, *Phys. Rev. A* **90**, 022111 (2014).
- [90] Q. Guan and R. J. Lewis-Swan, *Phys. Rev. Research* **3**, 033199 (2021).
- [91] L. Garbe, O. Abah, S. Felicetti, and R. Puebla, *Quantum Sci. Technol.* **7**, 035010 (2022).
- [92] T. Caneva, R. Fazio, and G. E. Santoro, *Phys. Rev. B* **78**, 104426 (2008).
- [93] R. Puebla, S. Deffner, and S. Campbell, *Phys. Rev. Research* **2**, 032020 (2020).
- [94] O. Abah, G. De Chiara, M. Paternostro, and R. Puebla, *Phys. Rev. Research* **4**, L022017 (2022).
- [95] J. Vidal, S. Dusuel, and T. Barthel, *J. Stat. Mech. Theory Exp.* **2007**, P01015 (2007).
- [96] J. Wilms, J. Vidal, F. Verstraete, and S. Dusuel, *J. Stat. Mech. Theory Exp.* **2012**, P01023 (2012).
- [97] G. D. Chiara and A. Sanpera, *Rep. Prog. Phys.* **81**, 074002 (2018).
- [98] J. Bao, B. Guo, H.-G. Cheng, M. Zhou, J. Fu, Y.-C. Deng, and Z.-Y. Sun, *Phys. Rev. A* **101**, 012110 (2020).
- [99] M.-L. Hu, F. Fang, and H. Fan, *Phys. Rev. A* **104**, 062416 (2021).
- [100] J. Bao, Y.-H. Liu, and B. Guo, *J. Phys.: Condens. Matter* **33**, 495401 (2021).
- [101] S. Pilatowsky-Cameo, J. Chávez-Carlos, M. A. Bastarrachea-Magnani, P. Stránský, S. Lerma-Hernández, L. F. Santos, and J. G. Hirsch, *Phys. Rev. E* **101**, 010202 (2020).
- [102] K. Pal, K. Pal, and T. Sarkar, arXiv e-prints , arXiv:2204.06354 (2022), arXiv:2204.06354 [quant-ph].
- [103] A. Russomanno, F. Iemini, M. Dalmonte, and R. Fazio, *Phys. Rev. B* **95**, 214307 (2017).

- [104] M. Albiez, R. Gati, J. Fölling, S. Hunsmann, M. Cristiani, and M. K. Oberthaler, *Phys. Rev. Lett.* **95**, 010402 (2005).
- [105] T. Zibold, E. Nicklas, C. Gross, and M. K. Oberthaler, *Phys. Rev. Lett.* **105**, 204101 (2010).
- [106] J. Zhang, G. Pagano, P. W. Hess, A. Kyprianidis, P. Becker, H. Kaplan, A. V. Gorshkov, Z.-X. Gong, and C. Monroe, *Nature* **551**, 601 (2017).
- [107] J. A. Muniz, D. Barberena, R. J. Lewis-Swan, D. J. Young, J. R. K. Cline, A. M. Rey, and J. K. Thompson, *Nature* **580**, 602 (2020).
- [108] K. Xu, Z.-H. Sun, W. Liu, Y.-R. Zhang, H. Li, H. Dong, W. Ren, P. Zhang, F. Nori, D. Zheng, H. Fan, and H. Wang, *Sci. Adv.* **6**, eaba4935 (2020).
- [109] S. Dusuel and J. Vidal, *Phys. Rev. B* **71**, 224420 (2005).
- [110] E. Romera, M. Calixto, and O. Castaños, *Phys. Scr.* **89**, 095103 (2014).
- [111] D. Gutiérrez-Ruiz, D. Gonzalez, J. Chávez-Carlos, J. G. Hirsch, and J. D. Vergara, *Phys. Rev. B* **103**, 174104 (2021).
- [112] J. M. Radcliffe, *J. Phys. A: Gen. Phys.* **4**, 313 (1971).
- [113] W.-M. Zhang, D. H. Feng, and R. Gilmore, *Rev. Mod. Phys.* **62**, 867 (1990).
- [114] M. C. Gutzwiller, *Chaos in classical and quantum mechanics*, Vol. 1 (Springer Science & Business Media, 2013).
- [115] F. M. Izrailev, *Phys. Rep.* **196**, 299 (1990).
- [116] V. Kota, *Phys. Rep.* **347**, 223 (2001).
- [117] F. Evers and A. D. Mirlin, *Rev. Mod. Phys.* **80**, 1355 (2008).
- [118] P. Jurcevic, H. Shen, P. Hauke, C. Maier, T. Brydges, C. Hempel, B. P. Lanyon, M. Heyl, R. Blatt, and C. F. Roos, *Phys. Rev. Lett.* **119**, 080501 (2017).